Environmental Science Processes & Impacts

# $N_2O_5$ Reactive Uptake Kinetics and Chlorine Activation on Authentic Biomass-Burning Aerosol



| | |
|---|---|
| Journal: | *Environmental Science: Processes & Impacts* |
| Manuscript ID | EM-ART-07-2019-000330.R1 |
| Article Type: | Paper |
| Date Submitted by the Author: | 14-Sep-2019 |
| Complete List of Authors: | Goldberger, Lexie; Pacific Northwest National Laboratory,<br>Jahl, Lydia; Carnegie Mellon University, Chemistry<br>Thornton, Joel; University of Washington, Atmospheric Sciences<br>Sullivan, Ryan; Carnegie Mellon University, Chemistry; |
| | |

## Environmental Significance

Wildfires are a major and potentially growing impact on atmospheric composition, air quality, and climate. The large emissions of reactive trace gases, such as nitrogen oxide radicals, halogens, and particulate matter make the chemical evolution of wildfire smoke both fascinating and also necessary to understand the subsequent downstream impacts on secondary pollutants that impact human and ecosystem health as well as Earth's energy balance.

# $N_2O_5$ Reactive Uptake Kinetics and Chlorine Activation on Authentic Biomass-Burning Aerosol

Lexie Goldberger[1,†], Lydia G. Jahl[2], Joel A. Thornton[1,*], and Ryan C. Sullivan[2,*]

[1]Department of Atmospheric Science, University of Washington, Seattle, WA, USA
[2]Center for Atmospheric Particle Studies, Carnegie Mellon University, Pittsburgh, PA, USA
[†]Now at: Pacific Northwest National Laboratories, Richland, WA, USA
*Corresponding Authors: Joel Thornton (thornton@atmos.washington.edu); Ryan C. Sullivan (rsullivan@cmu.edu)

## Abstract

We examined the reactive uptake of dinitrogen pentoxide ($N_2O_5$) to authentic biomass-burning aerosol (BBA) using a small chamber reservoir in combination with an entrained aerosol flow tube. BBA was generated from four different fuel types and the reactivity of $N_2O_5$ was probed from 30 to 70% relative humidity (RH). The $N_2O_5$ reactive uptake coefficient, $\gamma(N_2O_5)$, depended upon RH, fuel type, and to a lesser degree on aerosol chloride mass fractions. The $\gamma(N_2O_5)$ ranged from 2.0 (±0.4) $x10^{-3}$ on black needlerush derived BBA at 30% RH to 6.0 (±0.6) $x10^{-3}$ on wiregrass derived BBA at 65% RH. Major $N_2O_5$ reaction products were observed including gaseous $ClNO_2$ and $HNO_3$ and particulate nitrate, and used to create a reactive nitrogen budget. Black needlerush BBA had the most particulate chloride, and the only measured $ClNO_2$ yield > 1%. The $ClNO_2$ yield on black needlerush decayed from an initial value of ~100% to ~ 30% over the course of the burn experiment, suggesting a depletion of BBA chloride over time. Black needlerush was also the only fuel for which the reactive nitrogen budget indicated other N-containing products were generated. Generally, the results suggest limited chloride availability for heterogeneous reaction for BBA in the RH range probed here, including BBA with chloride mass fractions on the higher end of reported values (~17-34%)(1,2). though less than sea spray aerosol, ~50%(3). We use these measured quantities to discuss the implications for nocturnal aerosol nitrate formation, the chemical fate of $N_2O_5$ (g), and the availability of particulate chloride for activation in biomass burning plumes.

## 1. Introduction

Biomass burning (BB) is a global scale phenomenon with a natural component that is expected to increase in frequency and intensity with a warming climate(4). BB represents a significant source of aerosol particles and reactive nitrogen that influence air quality and climate(5–7). Nitrogen oxide radicals ($NO_x = NO + NO_2$) are produced by the medium temperature combustion of the biomass that liberates nitrogen contained in the fuel(8,9). $NO_x$ has a crucial role in regulating the troposphere's oxidizing capacity(10–12). Biomass-burning aerosol (BBA) is also a potentially large inland source of particulate chloride(1,13–15), which if activated into photolabile chlorine-atom reservoirs could have an additional impact on the regional oxidant budgets rarely incorporated in studies of BB effects on atmospheric chemistry(16). A major type of biomass fuel burned

in North America and globally are tall grasses and shrubs, which also tend to have higher chloride concentrations than other types of flora(17–19). BBA derived from natural flora are reported to have mass fractions of chloride between 0 and 34%, and the fuels selected for this study reflect the extent of this range(2).

At night, $NO_2$ reacts with $O_3$ to form $NO_3$ (g), which subsequently reacts either with certain volatile organic compounds (VOC) or $NO_2$, the latter reaction producing dinitrogen pentoxide, $N_2O_5$, the mechanism of which is described here (12,20,21). In the absence of reactions on aerosol particles, $N_2O_5$ extends the lifetime of $NO_x$ until sunrise when $NO_3$ photolysis and reaction with NO causes the loss of $N_2O_5$ via thermal equilibrium. $N_2O_5$ reactions on aerosol particles are known to produce $HNO_3$ and nitryl chloride, $ClNO_2$, among other possible products(22,23). $ClNO_2$ promptly evaporates following aerosol-phase production, and photolyzes the subsequent day to release a chlorine atom while recycling $NO_x$. Cl atoms react rapidly with methane and other hydrocarbons(24–27) and $NO_x$ regulates $HO_x$ abundance. As such, $ClNO_2$ production contributes to the oxidizing capacity of the atmosphere. A common mechanism for $N_2O_5$ multi-phase chemistry is summarized in R1 – R8, and the relevant overall reaction in R9:

$$NO_2(g) + NO_3(g) \Leftrightarrow N_2O_5(g) \quad [R1]$$
$$N_2O_5(g) \Leftrightarrow N_2O_5(p) \quad [R2]$$
$$N_2O_5(p) \Leftrightarrow NO_3^-(aq) + NO_2^+(aq) \quad [R3]$$
$$NO_2^+(aq) + H_2O(p) \rightarrow H^+(aq) + HNO_3(aq) \quad [R4]$$
$$NO_2^+(aq) + Cl^-(aq) \rightarrow ClNO_2(aq) \quad [R5]$$
$$NO_2^+(aq) + X(aq) \rightarrow \text{Products} \quad [R6]$$
$$ClNO_2(aq) \Leftrightarrow ClNO_2(g) \quad [R7]$$
$$ClNO_2(g) + h\nu \rightarrow Cl(g) + NO_2(g) \quad [R8]$$
$$N_2O_5(g) + \text{particles} \rightarrow \phi ClNO_2 + (2-\phi)\, HNO_3 \quad [R9]$$

The above mechanism is a summary of insights developed from experiments demonstrating that multiple aerosol properties affect $N_2O_5$ reactive uptake kinetics and product yields, and the branching ratio between $ClNO_2$ and $HNO_3$ production, denoted as $\phi$. X (R6) represents species other than $H_2O$ and $Cl^-$, such as iodide and phenols, which can react with the short-lived $NO_2^+$ intermediate in tropospheric aerosol particles. First, in cases of low relative humidity, lower liquid water content reduces the rate of $N_2O_5$ reactive uptake, presumably at the ionization step to form a hydrated $NO_2^+$ intermediate(28,29). This reduction in rate also applies for solid particles devoid of liquid water(30). Second, nitrate in the particle can reduce the net reactive uptake of $N_2O_5$ by an order of magnitude through what is known as the nitrate effect (R3)(31–33). Third, particulate chloride can enhance $N_2O_5$ uptake, potentially canceling the nitrate suppression effect(33), and leading to $ClNO_2$ formation at the expense of inorganic nitrate formation. The ratio of reaction rates for the $NO_2^+$(aq) intermediate with $Cl^-$

relative to $H_2O$, $k_5/k_4$, has been found to range from ~500 to 800(33–35). Additionally, organic carbon coatings on aerosol particles reduce $N_2O_5$ uptake, most likely because they reduce the available water in the surface region of the aerosol, limiting the $N_2O_5$ ionization rate (R3), as well as its solubility and diffusivity through the particle(36,37).

The yield of $ClNO_2$ can also be affected by aerosol composition, namely due to competition between the chloride and other nucleophiles that react with the $NO_2^+$ intermediate from $N_2O_5$ hydrolysis(33,38,39). To date, the formation rates of only $HNO_3$ and $ClNO_2$ have been quantified, while nitration of condensed phase organics has been identified but the rate (and thus yield) remain uncertain for atmospheric aerosol(38,39). As noted in Thornton et al. (2003), the above sequential steps may well occur as a concerted one-step process where the transition state is a hydrated (or otherwise stabilized) $N_2O_5$ interacting with a nucleophile such as $H_2O$ or $Cl^-$(29).

Additionally, another pathway through which chlorinated species may partition in and out of the aerosol is by acid displacement of $Cl^-$ as HCl (g)(40). HCl equilibrium partitioning to aerosol particles is set by aerosol water content and pH, and in the gas-phase, HCl can be oxidized by hydroxyl radicals (OH) to generate chlorine atoms(41). For biomass burning, the presence of nitric acid ($HNO_3$) produced by $NO_x$ oxidation, e.g. (R4), could contribute to this acid-displacement chemistry(42). Similar chloride depletion has been observed in wildfires smoke influenced aerosol(15) and in our previous smog chamber experiments using authentic BBA(14).

The extent of heterogeneous and multiphase chemical processing that occurs in authentic BBA is largely unexplored and thus highly uncertain. The above drivers of $N_2O_5$ reactant and $ClNO_2$ or other product formation are essentially all present within BBA due to the significant production of nitrogen oxides from the fuel(6,9). BBA from certain fuels are rich in inorganic chloride(1,17,18), yet always contain a significant fraction of organic material which can potentially reduce $N_2O_5$ reactivity by lowering the overall liquid water content or availability(37), or be potential sites for $N_2O_5$ reaction via organic nitration. The high concentrations of VOC emitted also provide a large potential sink for the $NO_3$ radical that could inhibit the production and fate of $N_2O_5$(6,17,18). Since $NO_3$ is in thermal equilibrium with $N_2O_5$ (R3), reaction between the nitrate radical and VOCs can also deplete $N_2O_5$ that does form, without going through the aerosol reactive uptake pathway. However, in our prior chamber experiments simulating nocturnal chemistry of authentic BB smoke from various fuels, $N_2O_5$ was always produced immediately following the addition of moderate levels of ozone(14). This indicates that enough $NO_x$ and $NO_3$ remain in the diluted nascent smoke to produce $N_2O_5$, despite the large volatile organic component sink. In one study using ambient, aircraft measurements over the Southeast U.S. from the SENEX campaign, reaction of the nitrate radical with VOCs in a biomass burning plume were estimated to account for >99% of the $NO_3$+$N_2O_5$ loss(8).

Observations of $ClNO_2$ inland(43,44) suggest the potential for particle chloride sources other than sea spray participating in reactive chlorine cycling. As biomass-burning plumes contain the precursors necessary for $ClNO_2$ formation, they are good candidates to be studied in this regard(45). Moreover, improving poorly constrained interactions between BBA and $NO_x$, specifically by constraining the reactivity of $N_2O_5$ on BBA and the associated products, can therefore aid predictions of BBA chemical evolution and corresponding impacts on oxidative capacity, BBA optical properties, toxicity, hygroscopicity, and pH(46–50). In our prior chamber experiments, Ahern et al. demonstrated that nocturnal processing of biomass burning aerosol could produce $N_2O_5$ and then $ClNO_2$ with up to a 10% $N_2O_5$ to $ClNO_2$ conversion process and observed incomplete displacement of particulate chloride(14).

The experimental challenges of using authentic BBA to study $N_2O_5$ uptake kinetics and product yields on BBA have resulted in a gap in the literature for this type of experiment. Proxy aerosol composed of only organic components have typically been used to represent authentic BBA, which is different in composition and morphology(29,39,51). $N_2O_5$ reactive uptake kinetics are nonlinearly suppressed by the presence of organics or nitrate, or enhanced by chloride or particle liquid water content, so simple BBA proxies would potentially lead to results that do not accurately represent authentic BBA(27,33,37,52) that contains a complex mixture of black carbon, soot, minerals, inorganic salts, and organic carbon that are inhomogenously distributed at the single-particle level(53–57). Furthermore, particle composition, mixing state, and morphology vary between individual particles, fuel sources, combustion conditions, and extent of atmospheric processing(1,7,17,18,58,59). Herein, we describe the results from the first experiments to determine $N_2O_5$ reactive uptake and $ClNO_2$ production in authentic fresh BBA from a range of fuel types and at different RH, using an entrained aerosol flow reactor.

## 2. Experimental Methods

The experimental apparatus consisted of four components: a burn area and smoke reservoir, an $N_2O_5$ generation unit, an entrained aerosol flow reactor, and gas and particle characterization instruments. A schematic is shown in Figure 1.

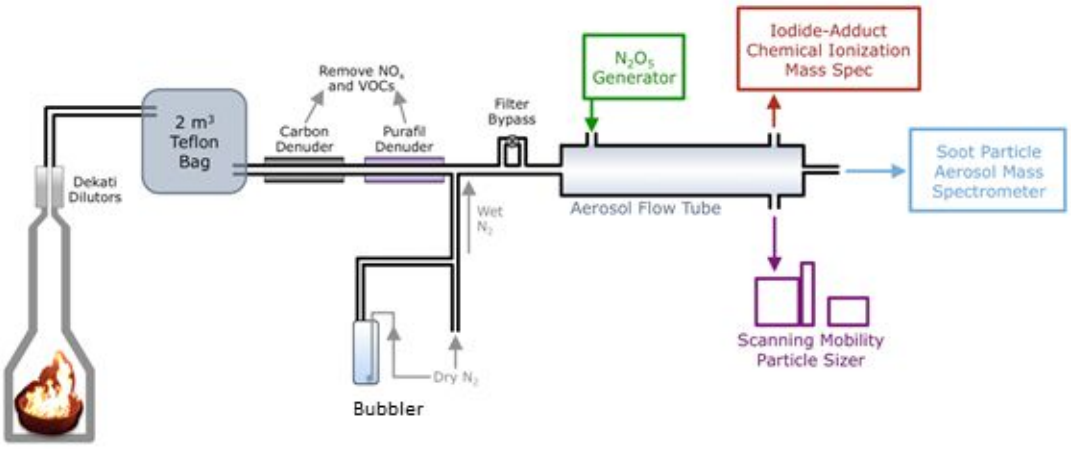


**Figure 1.** Entrained aerosol flow reactor schematic for biomass-burning aerosol kinetics experiments. The apparatus combines a combustion facility coupled to a Teflon reservoir chamber for the BBA, followed by an entrained aerosol flow reactor coupled to $N_2O_5$ (g) synthesis and delivery, and trace gas and particle sampling instrument.

## 2.1 Fuel Combustion

Four different fuel types were combusted: saw palmetto (*Serenoa repens*), wiregrass (*Aristida stricta*), black needlerush (*Juncus roemerianus*), and longleaf pine needles (*Pinus palustris*). The first three are grasses common to the southeastern U.S., and the longleaf pine is one of the major pine species in the southeastern U.S(2). Only smoke produced during the flaming stage was sampled into the smoke reservoir chamber. The saw palmetto and wiregrass were collected at Okefenokee National Wildlife Refuge in Georgia, the black needlerush was collected at Alligator River National Wildlife Refuge in North Carolina by students from Carnegie Mellon University, and the longleaf pine needles were purchased from an individual seller in Georgia. In these experiments, each fuel type was dried and stored in the open air in a clean lab space until use. The burn area and the dilution chamber were enclosed, without lights. Approximately 80 to 125 g of dried fuel were combusted for each experiment.

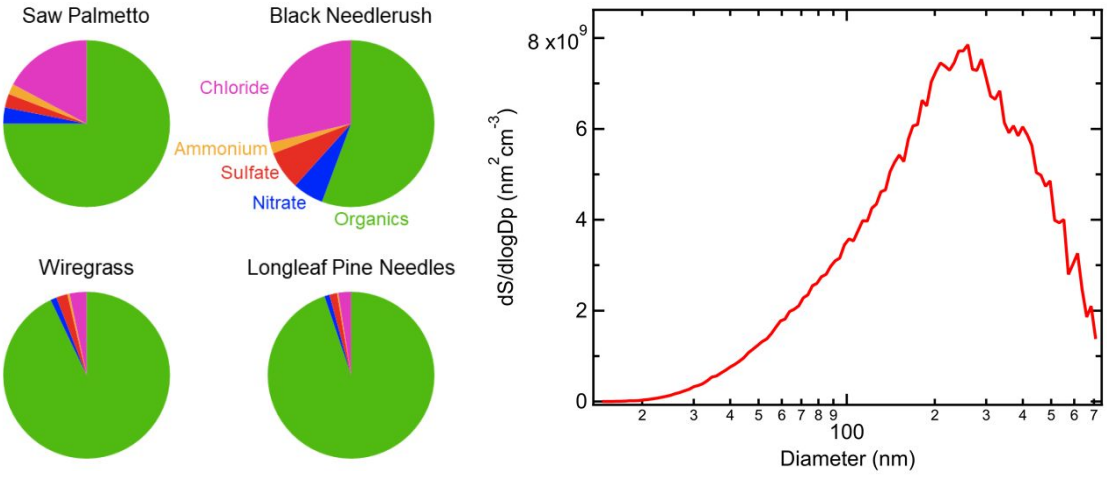


**Figure 2**. Biomass-burning aerosol non-refractory chemical composition (left) for the four biomass fuels studied here. The average composition shown here was determined with the SP-AMS at low RH, before addition of $N_2O_5$. Right: example aerosol surface area size distribution of wiregrass BBA at low RH (37%). The distributions shifted slightly over the course of each experiment, with the surface area mean diameter increasing about 15%.

## 2.2. BBA Generation, Delivery, and Characterization

Biomass fuel was combusted in a partially enclosed galvanized steel pan and the resulting emissions were passed through a Dekati educator diluter, which sent a portion of the smoke – including gas and particles – into one of the Carnegie Mellon University 2 $m^3$ PTFE smog chambers(14,49,60). The chamber was equipped to chemically process or physically age the combustion emissions under a myriad of conditions, including UV radiation. In this case, the chamber was used as a smoke reservoir to deliver a more constant BBA source to the entrained aerosol flow reactor. The chamber was kept dark to preserve the conditions of nocturnal chemistry. Between experiments when not in use the chamber was continuously exposed to UV lights and flushed with clean air, free of VOCs and particles. New experiments were not conducted until particle number concentrations reached <10 $cm^{-3}$ between experiments. The flow reactor apparatus was continuously flushed with clean air between experiments as well, and pre-experiment sampling from the flow reactor confirmed the system had been flushed thoroughly. Had $N_2O_5$ concentrations decreased over the course of the experiment, it could have been concluded that the flow tube was taking up BBA on its walls, but this was not observed.

After filling the chamber to an aerosol mass concentration of 200-250 $\mu g/m^3$ (estimated by the SMPS), 2 standard liters per minute (slpm) of BBA was continually drawn from the smoke chamber through the flow reactor by the combined instrumentation sampling from the flow tube. Between the chamber and the flow reactor, the aerosol transfer tubing was such that large particles (> 2 μm aerodynamic diameter) were impacted prior to or settled out of the flow reactor, leaving an authentic size distribution of BBA. Before reaching the flow reactor, the smoke-laden flow passed through a Purafil permanganate denuder and then a charcoal denuder to remove any $NO_x$ and VOCs, respectively, which could otherwise influence the $N_2O_5$ concentration in the flow reactor. The scrubbing efficiency of these denuders were checked in separate experiments using a commercial $NO_x$ monitor (Advanced Pollution Instrumentation, Inc. Model 200A, limit of detection 4 ppb) and a PTR-MS (Ionicon Analytic GmbH, limit of detection ~500 ppt with dependence on m/z) to measure VOCs. The scrubbing efficiencies were > 90% for $NO_x$ and > 95% for VOCs. Finally, before entering the flow reactor the smoke was humidified to either 30-40% or 60-70% relative humidity (RH) in a section of copper tubing prior to the kinetics flow reactor; an RH probe (Vaisala HMP233) was used to periodically check the RH at the end of the reactor.

BBA number size distributions and BBA bulk chemical composition were continuously measured at the exit of the flow reactor during an experiment using a Scanning Mobility Particle Sizer (SMPS; 3082 DMA and 3775 CPC, TSI Inc.) and a Soot-Particle Aerosol Mass Spectrometer (SP-AMS) with a standard inlet with a reported transmitted size range of 50-700 nm(61), respectively. Periodically the aerosol size distribution and composition were measured at the flow tube entrance for comparison.

**Table 1.** Experimental conditions, aerosol composition, and derived $N_2O_5$ reaction probability ($\gamma(N_2O_5)$) and $ClNO_2$ product yield ($\phi ClNO_2$) for entrained aerosol flow reactor experiments on BBA under low or high RH conditions. The uncertainty ($2\sigma$) reported here refers to the variability over the course of the experiment. The propagated measurement uncertainty is ±30% within an order of magnitude. The resulting non-refractory BBA composition as measured by an Aerodyne Aerosol Mass Spectrometer pre-experiment, before exposure to $N_2O_5$ (g), is listed in units of μg $m^{-3}$. The mass fractions of species are written as percentages in parentheses. The calculated values of $\gamma(N_2O_5)$ and $\phi(ClNO_2)$ account for the diminishing concentrations measured over the course of the experiment.

| **BBA Fuel or Particle Type** | **RH** (%) | **Organics** [μg $m^{-3}$] (mf %) | **Nitrate** [μg $m^{-3}$] (mf %) | **Sulfate** [μg $m^{-3}$] (mf %) | **Ammonium** [μg $m^{-3}$] (mf %) | **Chloride** [μg $m^{-3}$] (mf %) | **$\gamma(N_2O_5)$** ($2\sigma$) x$10^{-3}$ | **$\phi ClNO_2$** ($2\sigma$) (%) |
|---|---|---|---|---|---|---|---|---|
| Saw Palmetto | 40 | 48 (75%) | 2 (3.1%) | 1.7 (2.7%) | 1.3 (2.0%) | 11 (17%) | 3.2 (0.4) | < 1 (2) |
| Saw Palmetto | 60 | 49 (72%) | 1.7 (2.5%) | 2.6 (3.8%) | 1.7 (2.5%) | 13 (19%) | 3.6 (1) | < 0.5 (1.5) |
| Wiregrass | 37 | 85 (93%) | 1.1 (1.2%) | 2 (2.2%) | 0.4 (0.4%) | 3 (3.3%) | 2.8 (0.6) | ND |
| Wiregrass | 60 | 29 (89%) | 0.9 (2.8%) | 0.6 (1.8%) | 0.2 (0.6%) | 2 (6.1%) | 6 (0.6) | ND |
| Black Needlerush | 34 | 68 (56%) | 7.3 (6%) | 9.2 (7.5%) | 2.6 (2.0%) | 35 (29%) | 2.1 (0.4) | 6 (2) |
| Black Needlerush | 76 | 135 (75%) | 5.4 (3.0%) | 9.3 (5.1%) | 1.9 (1.1%) | 29 (16%) | 4.1 (0.2) | 50 (9) |
| LL Pine Needles | 30 | 77 (95%) | 0.8 (1.0%) | 1.2 (1.5%) | 0.2 (0.3%) | 2 (2.5%) | 3.2 (0.4) | ND |
| LL Pine Needles | 76 | 126 (96%) | 1.2 (0.9%) | 1.2 (0.9%) | 0.5 (0.4%) | 3 (2.3%) | 2.5 (0.4) | ND |

Typical aerosol size distributions and non-refractory chemical composition from experiments at low RH are shown in Figure 2. While the IR laser in the SP-AMS was switched on and off in some experiments, to increase the number of measurements available we focused on IR-off mode measurements, that measure the non-refractory aerosol components and not black carbon/soot. BBA surface area concentrations in the flow tube typically ranged from 0.5 to 2.0 x$10^4$ $\mu m^2$ $cm^{-3}$, and generally decreased with time throughout the experiment as the smoke dilution chamber was depleted and diminished in volume. Aerosol settling along with wall losses likely contributed to diminishing concentrations in the chamber as well. Independent of fuel type, organics dominated the non-refractory mass of BBA studied throughout the course of their evolution (Table 1). Sulfate, ammonium, and chloride (contributions from both inorganic chloride salts and organic chlorine) tended to be less than 10% of BBA particle mass.

### 2.3. $N_2O_5$ Generation & Calibration

The online $N_2O_5$ source used in these experiments is the same as that described in Bertram et al(33). $NO_2$ from a calibrated cylinder (10 ppm $NO_2$ in $N_2$, purchased from Valley National Gases, labeled as a certified mixture) reacted with an excess of ozone in a fixed volume to produce a steady-state source of $N_2O_5$(g) through (R1). The

concentration of $N_2O_5$ in the flow reactor was typical of other studies of $N_2O_5$ reactive uptake but potentially an order of magnitude higher than what might be found in BB plumes at night(8). Online sampling of the trace gas species near a fresh, authentic plume is logistically difficult and observed values are limited. The amount of $N_2O_5$ produced was calibrated previously using a cavity ring down spectrometer three months before experiments were performed(62,63). $ClNO_2$ for calibration was produced using the $N_2O_5$ generator and passed over a neutral pH aqueous NaCl salt bed where a unit conversion of $N_2O_5$(g) to $ClNO_2$(g) is assumed(24,34,35,64,65). A small amount of $HNO_3$ was produced, on order of 100 pptv, which is near impossible to avoid in the humid environment of the salt slurry, and biases our calibration factor low by 8%, within the magnitude of measurement error. For calibration of the CIMS measurement of $N_2O_5$ or $ClNO_2$ the generated outflow was directly sampled at the CIMS inlet.

**2.4. Entrained Aerosol Flow Reactor Apparatus**

The aerosol flow reactor apparatus consisted of a 90 cm long pyrex tube with an inner diameter of 9 cm, the inner walls of which were coated with halocarbon wax(37). At the flow tube entrance, BBA from the chamber and $N_2O_5$ entered through separate, orthogonal 1 cm O.D. ports. Just upstream of the flow reactor entrance were the denuders, then the RH conditioning tube, and then a Teflon membrane filter unit. The aerosol flow drawn from the chamber either passed through the filter, to remove BBA, or bypassed the filter through a separate tubing line to allow BBA to enter the flow reactor. A total flow rate of 2.0 slpm from the combined instrumentation was used to draw BBA from the chamber through the flow reactor. The residence time in the flow tube was 2 minutes with a Reynolds number of 32 indicating laminar flow. The reactor was maintained at room temperature and atmospheric pressure.

**2.5. Gas-phase Measurements**

Throughout the experiment, commercial chemiluminescence and UV absorption instruments continuously monitored $NO_x$ (Advanced Pollution Instrumentation, Inc. Model 200A) and $O_3$ (Dasibi Environmental Corp. Model 1008-PC). An HR-LToF-CIMS using iodide adduct ionization allowed for the monitoring of HCl, $HNO_3$, $N_2O_5$, and $ClNO_2$, among other gases. The CIMS was calibrated for HCl and $HNO_3$ via permeation tubes that had been continuously heated to 40 °C with air flowing over them, measured and weighed over the course of the year preceding the experiment. The output of the $N_2O_5$ generator was calibrated prior to the campaign as described in Lee et al(65). The sampling and ionization region was similar to that described by Lee et al(66), while the LToF-MS (Tofwerk AG) provides mass resolving power (m/Δm) of ~ 10,000. Iodide ions are generated by flowing trace methyl iodide vapor from a permeation tube in dry $N_2$ through a $^{210}P$ 10 mCi radioactive source. All trace gases reported here were detected as the corresponding cluster with iodide. As the clustering efficiency is known to scale

nonlinearly with water vapor, the flow into the CIMS inlet was supplemented with a humidified flow to keep the relative humidity constant in the ion molecular region. The CIMS ion signal was calibrated versus the concentration of $N_2O_5$ or $ClNO_2$ using the calibrant generation described above. Further details regarding CIMS operation are found in Ahern et al(14).

### 2.6 Determination of $k_{het}$, $\gamma$, and $\phi$

The rate of change of $N_2O_5$ and products such as $ClNO_2$ and $HNO_3$ due to $N_2O_5$ reactive uptake to BBA can be described by equations 1 to 3:

$$\frac{d[N_2O_5]}{dt} = -k_{het}[N_2O_5] \quad [1]$$

$$\frac{d[ClNO_2]}{dt} = \phi k_{het}[N_2O_5] \quad [2]$$

$$\frac{d[HNO_3]}{dt} = (2-\phi)k_{het}[N_2O_5] \quad [3]$$

This system assumes the only reaction products are $ClNO_2$ and $HNO_3$, and thus $\phi$ represents the branching between these two products. The pseudo-first order reaction rate constant due to reactive uptake of $N_2O_5$ to BBA, $k_{het}$, can be written as equation 4, assuming minimal mass transfer limitations due to gas-phase diffusion, which is the case for the uptake efficiencies and particle sizes in these experiments(67,68).

$$k_{het} = \frac{\gamma_{N_2O_5}\omega S_a}{4} \quad [4]$$

In equation 4, $\gamma(N_2O_5)$ is the heterogeneous reaction probability, $\omega$ is the mean molecular speed of $N_2O_5$, and $S_a$ is the aerosol particle surface area per volume of air ($cm^2\ cm^{-3}$). Experiments were conducted using this simple framework in order to determine values of $\gamma(N_2O_5)$ and $\phi(ClNO_2)$.

The kinetic parameters $k_{het}$ and subsequently $\gamma(N_2O_5)$ were determined using the particle modulation technique described in Bertram et al(33). In this approach, interaction time between $N_2O_5$ and BBA is fixed, and $N_2O_5$ delivery is constant, while particle surface area in the flow reactor is periodically modulated between nearly zero to greater than ~ 2 x $10^3$ $\mu m^2\ cm^{-3}$ by means of a Teflon filter and filter-bypass between the smoke reservoir chamber and flow reactor (see Figure 1). While the filter was bypassed, BBA and any residual vapors making it through the denuders entered the flow reactor, and the $N_2O_5$ signal decreased. While the particle filter was inline, only the vapors passing through the denuders entered the flow reactor, and the $N_2O_5$ signal typically increased to a new steady-state concentration. The observation that $N_2O_5$ concentrations were higher while the aerosol surface area was near zero with the filter inline was consistent between all experiments.

Using the known residence time in the flow reactor ($\Delta t$), and the assumption that $N_2O_5$ reaction on the walls and aerosol particles is first-order, then the log of the

difference between $N_2O_5$ concentrations with and without aerosol particles present is proportional to $k_{het}$:

$$k_{het} = -(1/\Delta t)\ \ln([N_2O_5]^{w/particles}/[N_2O_5]^{wo/particles}) \quad [5]$$

The $\gamma(N_2O_5)$ can then be calculated by using the simultaneous observations of the BBA size distribution to obtain particle surface area concentrations, $S_a$ using equation 4. Thus, $\gamma(N_2O_5)$ is obtained by a linear fit of the $k_{het}$ values plotted versus $S_a$. The uncertainty in $\gamma(N_2O_5)$ was obtained by taking into the account the variance of $S_a$ and $k_{het}$ (via equation 4) and calculating the possible upper and lower limit from the observed variable range. For the small particle sizes (< 1μm) and generally small reactive uptake coefficients measured in our study, gas-phase diffusion is not a limitation in these experiments even at atmospheric pressure(26). The $\gamma(N_2O_5)$ derived is a value based on bulk reactivity. While a study as a function of aerosol size is warranted, it wasn't feasible with this apparatus due to limited concentrations of BBA.

To determine the $ClNO_2$ yield, $\phi$, $ClNO_2$ produced by $N_2O_5$ reaction on particles needs to be distinguished from $ClNO_2$ produced by reactions that occur on the flow reactor walls. Assuming the production efficiency of $ClNO_2$ at the reactor wall is constant and not dependent on the presence or absence of BBA in the flow reactor, we determined a $ClNO_2$ wall production efficiency using the observed ratio of $ClNO_2/N_2O_5$ when the particle filter was inline. Our assumption is supported by the fact that the background $ClNO_2$ in the absence of BBA is relatively constant across particle modulations. The wall-produced $ClNO_2$ is then subtracted from the total observed $ClNO_2$ concentration with BBA present to determine the $ClNO_2$ produced from the BBA only. The $\phi(ClNO_2)$ is then the ratio of $ClNO_2$ mole fraction produced on BBA ($\Delta ClNO_2$) to the $N_2O_5$ mole fraction having reacted on BBA ($\Delta N_2O_5$):

$$\phi\, ClNO_2 = \Delta ClNO_2/\Delta\, N_2O_5 \quad [6]$$

We scale the $ClNO_2$ mass spectral signal by a factor of 1.5 ± 0.07 relative to the $N_2O_5$ signal to account for a lower instrument response per mole of $ClNO_2$ as determined by CIMS calibrations performed immediately following the experiments.

**2.7 Control Experiments**

Control experiments were conducted to validate the heterogeneous kinetics obtained from the experimental apparatus. First, we used deliquesced ammonium bisulfate (ABS) aerosol particles at 55% RH, on which the reactive probability of $N_2O_5$ has been well documented(31-33) in place of BBA. An ABS solution in milliQ water was atomized and passed through the RH conditioning tube at 55% RH, and then into the flow reactor, downstream of the smoke chamber but upstream of the impactor and gas scrubbers. The size distributions of ABS particles were similar to those obtained in the flow reactor during the biomass burning experiments, with a geometric mean diameter of

205 ± 30 nm and initial concentration of $2.3 \times 10^2$ μg/m$^3$. The reaction probability of $N_2O_5$ on the ABS aerosol (0.009 ± 0.004) was determined using the same perturbation method described above within literature values reported (0.005-0.03)(33).

Additional controls were conducted during the BBA reactive uptake experiments. We periodically stopped the delivery of $N_2O_5$ to the flow reactor and used the CIMS to determine reactor background concentrations of products such as $HNO_3$ and $ClNO_2$. We also routinely sampled BBA at the entrance and exit to the flow reactor with the SP-AMS to evaluate BBA losses through the flow reactor, which were negligible.

## 3. Results and Discussion

### 3.1 Biomass-Burning Aerosol Composition & Reactivity

The concentrations of the non-refractory particulate components measured by the SP-AMS between biomass fuel types are shown in Table 1 and the component mass fractions are displayed in Figure 2. Due to the authenticity of the fuel, the aerosol concentrations of individual species vary from burn to burn, and the mean value across experiments of the same fuel type is used in the following discussion. Saw palmetto and black needlerush were considered the high chloride aerosol species with mass fractions of 18 and 22% respectfully, while wiregrass and longleaf pine needles had chloride mass fractions of 4.7 and 2.4%. These chloride fractions are all within the range reported in McMeeking et al. (2009) and Levin et al. (2010)(1,2), except for black needlerush in our experiments which contained more chloride, perhaps due to the location where it was collected in coastal North Carolina. Black needlerush as well had the highest fractions of particulate nitrate (4.5%) and sulfate (6.3%), greater by nearly a factor of four compared to the three other fuel types, while also containing the least organic carbon by mass fraction. Wiregrass and longleaf pine needles were dominated by the organic components with mass fractions of 91% and 95%.

An example time series of reactants and products are shown in Figure 3 from an experiment using BBA produced from saw palmetto fuel. After BBA concentrations reached steady state in the flow tube, $N_2O_5$ was introduced and allowed to stabilize. In the first mode of operation, a Teflon filter was placed inline just before the entrance to the flow tube to allow residual gases from the smoke to enter but not the BBA. Observed aerosol surface area concentrations went to near zero and concentrations of $N_2O_5$ increased. The aerosol flow was switched between filtered and bypass modes six times before proceeding to the next operational mode. In the second mode of operation, smoke input was kept constant in bypass mode while $N_2O_5$ addition into the flow tube was modulated on and off six times as well. When $N_2O_5$ was added to the flow tube, particulate nitrate ($pNO_3$) increased (Figure 3), $ClNO_2$ (g) increased (Figure 6), and particulate chloride (pCl) decreased (Figure 7).

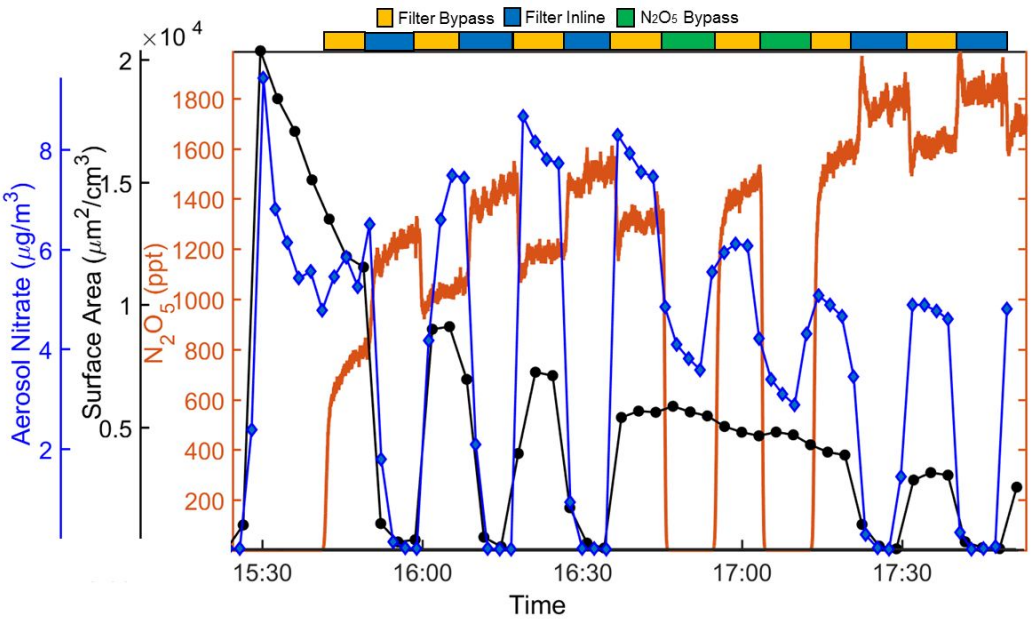


**Figure 3.** Exemplary $N_2O_5$ (g) (red line) reactive uptake experiment for black needlerush BBA at high RH (75%). BBA surface area (black circles) is modulated by passing the smoke through a filter or bypassing the filter into the flow reactor, indicated by the horizontal bar above. The $N_2O_5$ is continuously added to the chamber starting at 12:30, and the modulations of its signal are anti-correlated with the BBA abundance. Aerosol nitrate (blue diamonds) increases when BBA is present in the flow reactor with $N_2O_5$ versus when $N_2O_5$ delivery is stopped (yellow-green horizontal bar).

### 3.2 Determination of $N_2O_5$ Reaction Probability, $\gamma(N_2O_5)$

The natural logarithm of the ratio of $N_2O_5$ signal in the presence of BBA (bypass mode) to that in the absence of BBA (filtered mode) can be used with equations 4 and 5 to derive $\gamma(N_2O_5)$. Figure 4 shows this $N_2O_5$ signal ratio with and without BBA plotted versus BBA $S_a$, from the four different fuels, with each $N_2O_5$ experiment on each fuel type conducted under two different RH conditions of 35% and 75% (cyan and dark blue, respectively). The linear relationship ($R^2 > 0.8$) between the changes in $N_2O_5$ versus $S_a$ gives support for the interpretation that $N_2O_5$ is reacting with the aerosol surface area(52). The slope of the least-squares line of best fit, scaled by the flow tube residence time ($\Delta t$ = 120s), is directly proportional to $\gamma(N_2O_5)$ via equation 5.

The $\gamma(N_2O_5)$ on BBA from each fuel type displayed unique dependencies on BBA composition and RH. Table 1 summarizes the $\gamma(N_2O_5)$ measured for each fuel type, with values typically ranging from 2.0 to 6.0 $\times 10^{-3}$ across experiments. Saw palmetto BBA, with a non-refractory aerosol composition of 74% OA, 2% $pNO_3$, and 20% pCl, led to a $\gamma(N_2O_5)$ that increased slightly with RH, from 3.0 ± 0.4 $\times 10^{-3}$ at 35% RH to 4.0 ± 1.0 $\times 10^{-3}$ at 75% RH and exhibited the largest change in $pNO_3$ and $N_2O_5$(g) for both experimental operational modes, see Table 2. While saw palmetto BBA contained high levels of particulate chloride (18% by mass) compared to the other fuels ( 2-22%), the pCl changed relatively the least (-1 ± 0.1 μg $m^{-3}$, 10% of chloride mass) following exposure to $N_2O_5$. On both black needlerush BBA (22% pCl) and wiregrass BBA (4.7% pCl), $\gamma(N_2O_5)$ doubled between the low (34/37%) and high RH (60/76%) conditions,

from $2.0 \pm 0.4 \times 10^{-3}$ to $4.0 \pm 0.2 \times 10^{-3}$ and $3.0 \pm 0.6 \times 10^{-3}$ to $6.0 \pm 0.6 \times 10^{-3}$. Wiregrass BBA also exhibited the largest changes in pCl, a decrease of 23% chloride by mass or $-0.7 \pm 0.2$ μg $m^{-3}$, upon exposure to $N_2O_5$ at 60% RH, though $ClNO_2$ was not readily detected. For the pine needle BBA (2.4% pCl), $\gamma(N_2O_5)$ decreased slightly with elevated RH, from $3.0 \pm 0.4 \times 10^{-3}$ at 35% RH to $2.0 \pm 0.4 \times 10^{-3}$ at 75% RH and had the least change in $pNO_3$ for both experimental modes.

Regarding the gas-phase products of this reaction, it is likely the $N_2O_5$ was predominantly yielding $HNO_3$; however, given the significant memory effects of $HNO_3$ in the reactor, we do not attempt to interpret its instantaneous concentration as a measure of reaction branching. We might have expected pCl to change based on the displacement of HCl by $HNO_3$. Indeed, in the wiregrass BBA experiment pCl decreased significantly and $ClNO_2$ was not observed, presumably due to acid displacement. We were unable to conclusively detect HCl in these experiments, but note it could be present below our detection limit (~0.5 ppbv(65)). The quantitative measurement of HCl using iodide adduct is challenging, as it is a weak cluster, sensitive to small instrumental electric fields, and especially difficult in the presence of high water vapor, which leads to an overlapping ion(66).

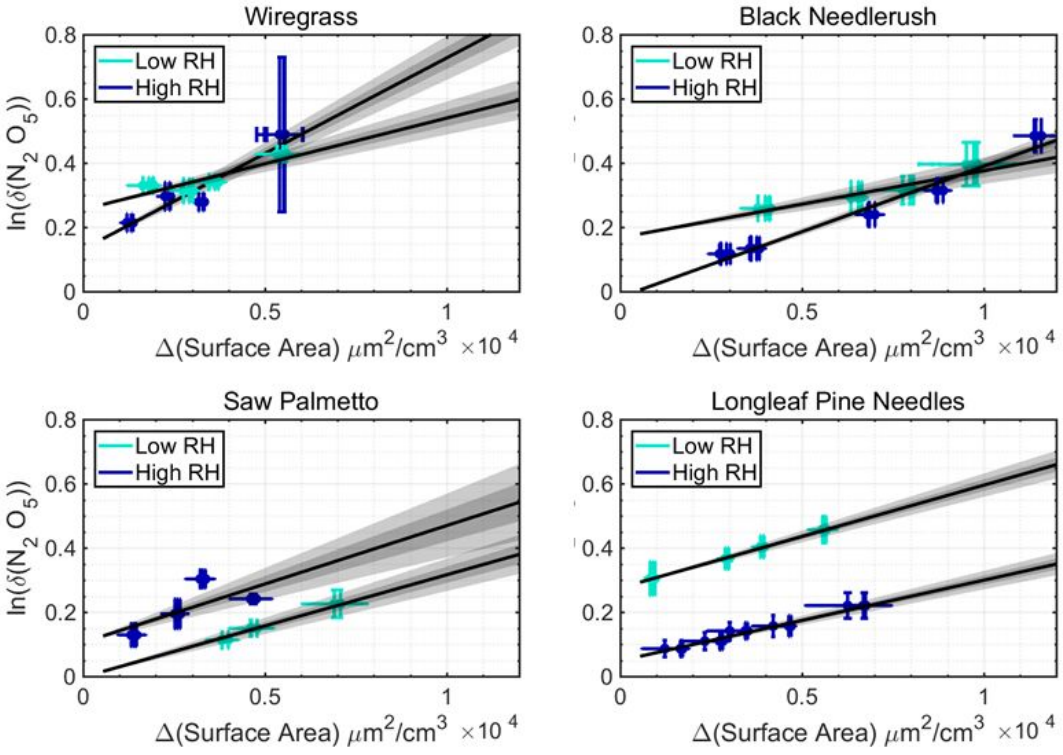


**Figure 4.** Determination of the reaction probability of $N_2O_5$ (g), $\gamma(N_2O_5)$, on the four types of BBA under low and high RH conditions. The natural log of the $N_2O_5$ signal ratio with and without BBA present in the flow reactor is plotted versus BBA surface area concentration measured in the flow reactor for low (cyan) and high (dark blue) RH, and four different fuels: wiregrass (top left), black needlerush (top right), saw palmetto (bottom left) and longleaf pine needles (bottom right). The error bars correspond to the uncertainties related to the variability over the course of each individual experiment. The slopes of the best fit lines are proportional to $\gamma(N_2O_5)$ via equations 4 and 5, and the gray shading shows uncertainty bounds derived from the regression from the absolute uncertainty in the underlying variables. The trendline equations are as follows: wiregrass, 37% RH: y = 2850 ± 260 *x + 0.25; wiregrass, 60% RH: y=6270 ± 340 *x + 0.12; black needlerush, 34% RH: y= 2200 ± 210*x + 0.16; black needlerush, 76% RH: 4130 ± 120*x – 0.02; saw palmetto, 40% RH: y= 3500 ± 250*x -0.02; saw palmetto, 60% RH: y=3820± 500*x +0.1; longleaf pine needles, 30% RH: y= 3250± 180*x + 0.27; long leaf pine needles, 76% RH: y= 2670 ± 140*x + 0.04

### 3.3 $\gamma(N_2O_5)$ compared to aerosol composition and other aerosol systems

No obvious trends in $N_2O_5$ reactivity with bulk non-refractory BBA composition were found, however, the expected roles of particulate organic aerosol and $pNO_3$ in the suppression of $\gamma(N_2O_5)$ compared to pure aqueous salt solutions were likely operational in the BBA. Wiregrass and pine needle BBA had the highest organic mass fraction (>90%) and a higher initial nitrate to chloride ratios at 0.3 and 0.4, respectively, compared to the other fuel types, and experienced the least change in $pNO_3$ upon $N_2O_5$ exposure, a 70 ± 16% and 50 ± 8% increase. Saw palmetto BBA exhibited the largest change in $pNO_3$, 159 ± 19% increase and lowest change in pCl, a decrease of 4 ± 12%, compared to BBA from the other fuel types. Black needlerush BBA had a smaller $pNO_3$ change with $N_2O_5$ exposure, 87 ± 11%, consistent with a large yield of $ClNO_2$.

The values of $\gamma(N_2O_5)$ derived in this experiment fit well within the context of previous literature values (Figure 5). The $\gamma(N_2O_5)$ on soot aerosol have been reported

between 2 x $10^{-4}$ and 0.03[83]. The $\gamma(N_2O_5)$ reported for mixed organic/inorganic aerosol ranges between 3 x $10^{-4}$ and 8.3 x $10^{-3}$ for humic acid mixed with aqueous ammonium sulfate at 6 to 40% by mass(69), and from 0.003 to 0.025(37) for organic mass fractions from 0 to ~50% using OA with a range of oxidation state. In the absence of organics, $pNO_3$ and pCl can affect $\gamma(N_2O_5)$ on aqueous inorganic particles. Aqueous inorganic $pNO_3$ generally suppresses $\gamma(N_2O_5)$(31), while aqueous pCl can compete with $pNO_3$ and offset its suppression(33,39). The significant mass fractions of OA in all the BBA studied here, and the moderate hygroscopicity of the fresh and thus low-oxidation state BBOA(70) likely explain the relatively low $\gamma(N_2O_5)$(36,37) compared to values of order 0.03 measured on aqueous ammonium bisulfate particles.

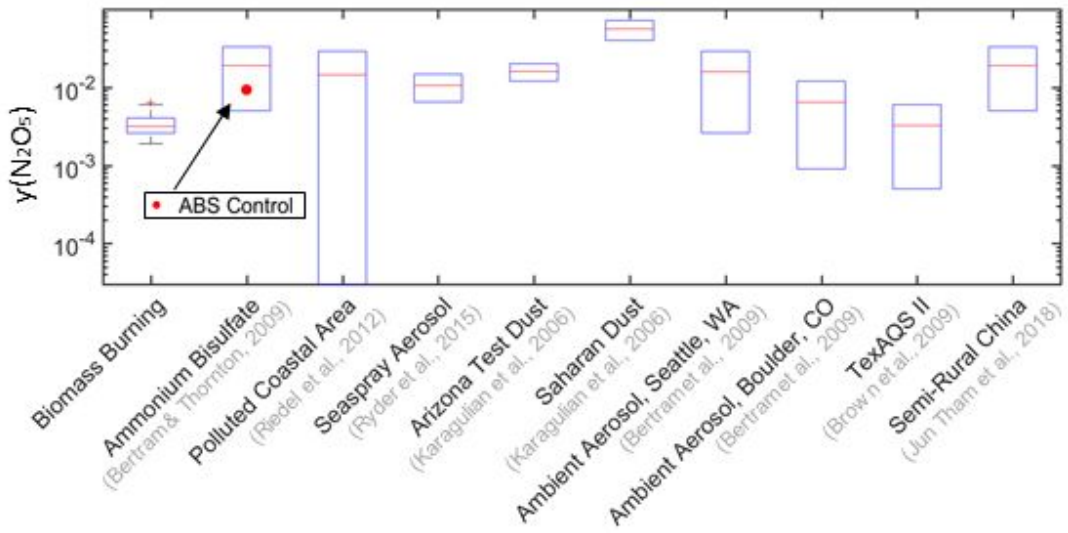


**Figure 5.** Values of $\gamma(N_2O_5)$ derived from this experiment on four types of BBA under low and high RH conditions, compared to reported values from experiments on other aerosol types, and ambient measurements. The values from biomass burning aerosol are at the lower end compared to the other aerosol types reported. The control ammonium bisulfate aerosol from this experiment (red circle) is within range of other reports.(33,39,71–75)

The suppression of the $\gamma(N_2O_5)$ relative to aqueous particles for the large amount of OA in these experiments is less than that expected based on experiments using humic acid and monoterpene SOA(36,69), possibly because the OA is not uniformly coating all the BBA particles and/or is more hygroscopic(37). Electron microscopy measurements conducted on BBA generated from the same fuels used in this experiment reveal salt particles with organic coatings surrounding the salt to different extents, which will be elaborated on in a future paper. Furthermore, the hygroscopicity of BBA is known to vary greatly, with kappa hygroscopicity parameter values ranging from low ($\kappa$=0.02-0.06) to very high ($\kappa$=0.6-0.8)(76,77). Some BB experiments have reported kappas as high as $\kappa$=1 with bimodal kappa distributions, further showing the wide variance of several properties of BBA that may impact $\gamma(N_2O_5)$(78).

In addition, while we have attempted to remove and minimize $NO_3$ radical reactivity from the smoke via the addition of VOC and $NO_x$ scrubbers and operating at high $NO_2$ (excess from the $N_2O_5$ generator), which suppresses $NO_3$ availability via $N_2O_5$ formation, we cannot guarantee the complete absence of $NO_3$ nor its reactivity in the flow tube. For $N_2O_5$ to be present $NO_3$ must also be available due to their thermal equilibrium (R1), and thus $NO_3$ reactivity also increases the apparent loss rate of $N_2O_5$. Therefore, our $\gamma(N_2O_5)$ values for BBA are likely biased high, as (1) $NO_3$ reactivity cannot be eliminated, and (2) the aerosol surface area measured by the SMPS is a lower estimate due to a maximum observable particle diameter of around 710 nm. As shown in Figure 2, the tail of the aerosol size distribution does extend past 710 nm in some BBA experiments. As noted above, a PTR-MS attached to the flow reactor did not measure significant concentrations of VOC that react with $NO_3$, indicating that most VOCs were removed prior to entering the flow tube. This suggests that little but not necessarily zero $NO_3$ reactivity through reaction with VOCs occurred in the flow reactor.

### 3.4 Chlorine activation and $ClNO_2$ production

An example time series of chlorine activation during the black needlerush BBA experiment at 75% RH is shown in Figure 6. $ClNO_2$ is not present until the addition of $N_2O_5$ into the flow reactor. Once $N_2O_5$ is introduced, $ClNO_2$ is produced both in the presence and absence of BBA, implying production occurring on both BBA and wall surfaces. The background $ClNO_2$ produced on wall surfaces (inferred from when BBA was not present) was generally constant over the duration of the experiment, while the total $ClNO_2$ signal decreases as the BBA $S_a$ decreases over the course of the experiment and when BBA is absent due to the placement of the filter inline. This allows us to resolve the contribution to $ClNO_2$ production from wall chemistry versus from reaction of $N_2O_5$ with the BBA, by subtracting the constant $ClNO_2$ concentration measured in the absence of BBA.

The $ClNO_2$ enhancement due to BBA decays with time, suggesting that as the BBA ages in the reservoir chamber, pCl becomes less available for activation. Aging can

occur through the slow evaporation of semi-volatile organic and inorganic aerosol components that can then partition to the chamber Teflon walls. Oxidants and other reactants emitted or produced in the nascent smoke can also cause some amount of chemical aging, though well below the extent of photochemical aging typically experienced during atmospheric transport timescales of hours to days. In Ahern et al. unexposed BBA was measured directly from the chamber, while in this study all BBA sampling took place from the flow tube(14). Thus, fresh black needlerush BBA in the presence of $N_2O_5$ may be a major source of $ClNO_2$ production(14). In the other fuels studied, the $ClNO_2$ signal typically had a similar trend, but was detected at a much lower fraction of the reacted $N_2O_5$ than that shown in Figure 6. For example, for black needlerush BBA at 75% RH, $ClNO_2$ enhancements with the BBA accounted for >30% of the $N_2O_5$ signal difference with and without BBA present. But for BBA from other fuels, $ClNO_2$ enhancements rarely exceeded 1% of the $N_2O_5$ signal difference, or were not detectable such as for longleaf pine needle BBA and wiregrass BBA at RH <70%. The background corrected $ClNO_2$ enhancements in the presence of BBA relative to the loss of $N_2O_5$ are used to calculate $\phi(ClNO_2)$, shown in Table 1.

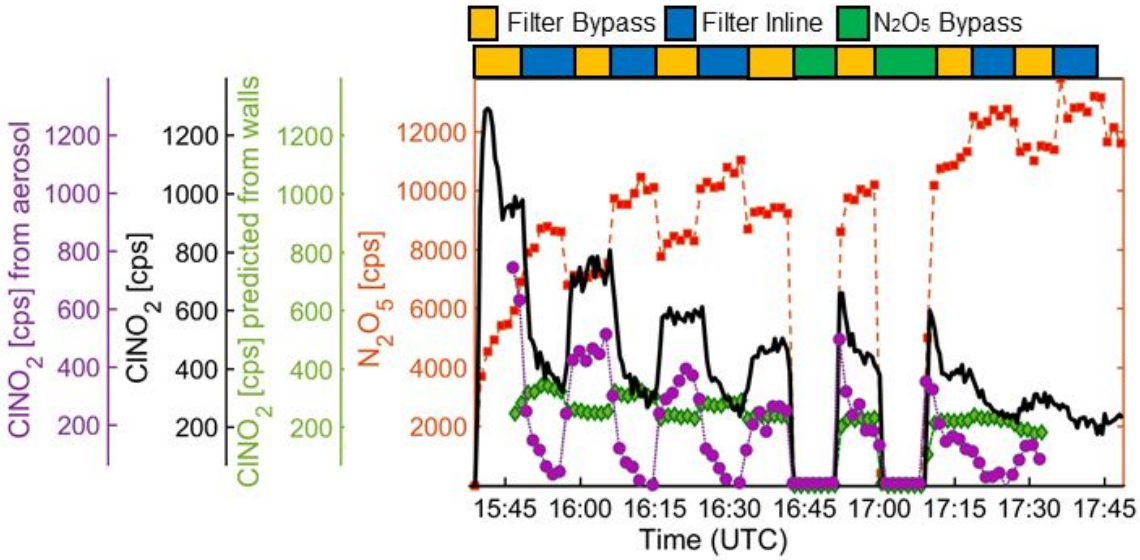


**Figure 6.** Observed production of $ClNO_2$(g) (black line) from $N_2O_5$(g) (red squares) reactive uptake to black needlerush BBA at high RH (75%), along with $ClNO_2$ production attributed to aerosol reactive (purple circles) uptake versus from the flow reactor walls (green diamonds). Periods with both $N_2O_5$ and BBA present in the flow reactor, indicated by the yellow bar, contain enhanced $ClNO_2$. Some $ClNO_2$ is continuously formed from $N_2O_5$ reacting on the walls of the flow reactor and transfer tubing. The amount of $ClNO_2$ from the walls (green) is determined from the periods when $N_2O_5$ is present in the flow tube without BBA (blue bar). The difference between the $ClNO_2$ signal measured when both BBA and $N_2O_5$ are present and that without BBA is the amount of $ClNO_2$ produced from $N_2O_5$ reacting on BBA (purple circles).

The exact reasons for the large range in $ClNO_2$ production efficiency on different types of BBA are not known at this time, but one possibility is related to particle chloride phase state and availability. The observed trend of efficient $ClNO_2$ production on the BBA with the highest pCl at the highest RH is reasonable. The most common chloride

salts present in BBA are KCl and $NH_4Cl$(1). KCl particles deliquesce at 85% RH and effloresce at 56%(28,79). Even in internally mixed particles, solid KCl may be present up to 82% RH(80). At the RH used in these experiments, it is thus quite possible the pCl was often in a solid form, inaccessible for aqueous chemistry, especially for all experiments with RH < 60%. While chloride activation from solid chloride particles has been documented(24,27), heterogeneous reaction rates are far slower than in aqueous systems, and $N_2O_5$ may well have additional reaction pathways in the complex BBA that outcompeted solid chloride interactions(26,28). Given that many wildfire plumes evolve during periods of relatively low humidity, this finding may have significant implications for the near-fire activation of chloride by $N_2O_5$ and the relative strengths of cycling versus sink processes of nitrogen oxides.

Previous exploration of $N_2O_5$ multiphase chemistry on authentic BBA that we presented in Ahern et al. used a 12 $m^3$ smog chamber with a mixing time of half an hour, exposing particles to $N_2O_5$ and water vapor for longer than the 2 minute residence time of these flow-tube experiments(14). In those chamber experiments $N_2O_5$ was produced from the nitrogen oxides present in the nascent smoke, plus the addition of ~80 ppb of ozone to the chamber. HCl was typically observed in the low hundreds of ppt. Estimates of $\gamma(N_2O_5)$ made using a box model were uncertain in that experiment, due to the role of turbulent mixing, long mixing times, and wall loss, but were consistent with our determinations here, in the range of $10^{-4}$–$10^{-2}$.

$ClNO_2$ production was observed more in our prior chamber experiments reported by Ahern et al. than in the flow reactor described here, and scaled with the mass fraction of particle chloride, though different fuel types were used in each experiment(14). The one fuel in Ahern et al. to exhibit a measurable yield of $ClNO_2$ was sawgrass (*Cladium jamaicense*)(14). Similar to black needlerush, sawgrass had elevated particulate chloride concentrations compared to the other fuels burned, and both species grow in coastal, marshy areas(14). $ClNO_2$ production in the chamber occurred after the formation of $N_2O_5$, and $ClNO_2$ concentrations continued to increase following the maximum in $N_2O_5$ concentration that was reached within 30 minutes following the addition of ozone. One reason for this difference could be the much longer interaction time in the chamber of more than 1.5 hours, allowing for more displacement and repartitioning of chloride across the size distribution, or to areas of the particles more accessible to $N_2O_5$, than the short two minutes interaction time in the flow reactor might allow. In addition, steam injection was used to facilitate mixing in the chamber and increase the chamber RH to a maximum of 60%, though small areas of the chamber may have exceeded 60% for short times during steam injection, possibly aiding in the deliquescence of KCl. The main conclusion is that for sawgrass and black needlerush, liberation of particulate chloride as $ClNO_2$ upon reactive uptake of $N_2O_5$ is highly likely.

### 3.5 Reactive Nitrogen Budget

The observed modulations of both gas and particle-phase nitrogen oxides can be used to evaluate the extent to which the measured products account for the amount of reactive nitrogen lost via $N_2O_5$ reactive uptake, as seen in Figure 7. Uncertainties in the absolute calibrations between $N_2O_5$, $HNO_3$, $ClNO_2$, and $pNO_3$, and differential losses of these components in the flow reactor apparatus prior to detection make such closure assessments challenging. For the species reported by the CIMS, an uncertainty of 30% is estimated for those directly calibrated(65). Our goal is to assess whether, given the inferred $\phi ClNO_2$ being in some cases ~ 0, we can infer other $N_2O_5$ reaction channels or unmeasured products. We evaluate the reactive nitrogen budget using equation 7:

$$\text{N balance} = 2 * \Delta N_2O_5(g) - (\Delta HNO_3(g) + \Delta ClNO_2 + \Delta pNO_3) \quad [7]$$

For each $N_2O_5$ that reacts in the flow reactor on aerosol particles, two N are converted into products, which will include $HNO_3$, $ClNO_2$, $pNO_3$, among other possible products not measured. A nitrogen balance of zero implies closure – all reacted $N_2O_5$ is accounted for by the measured products, whereas positive deviations from zero imply missing products, and negative deviations imply missing additional sources of the measured products.

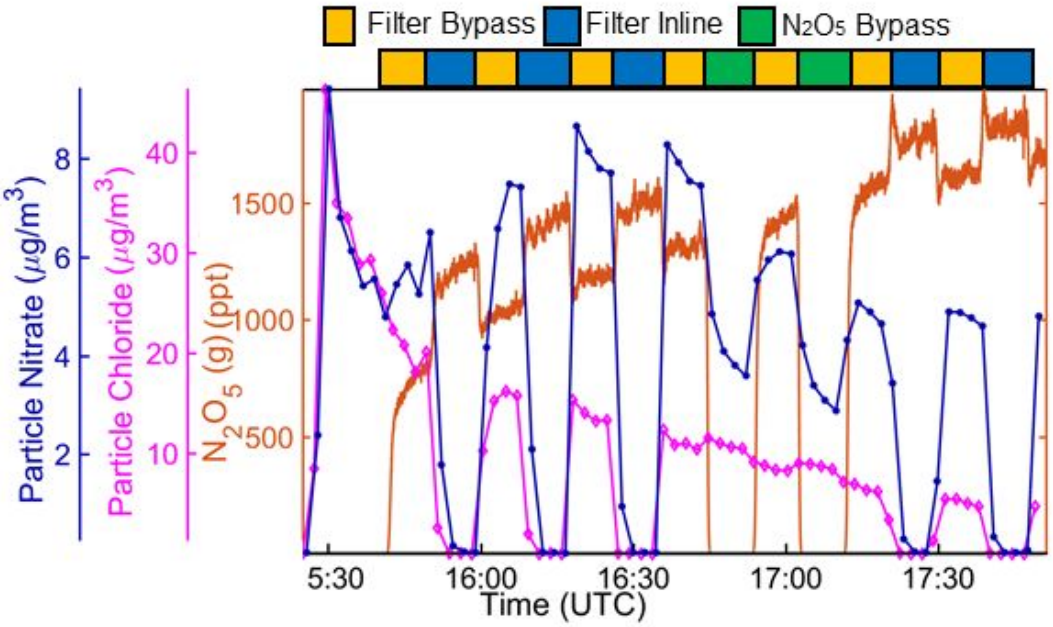


**Figure 7.** Time series of changes observed to black needlerush BBA particulate nitrate (dark blue circles) and chloride (pink diamonds) concentrations at high RH with and without exposure to $N_2O_5$(g) (red line) (yellow to green portion of horizontal bar). Observed particulate nitrate is strongly enhanced by the presence of $N_2O_5$, while particulate chloride is depleted to a lesser extent.

As illustrated in Table 2, most experiments resulted in an N balance between ± 50%, which, considering calibration uncertainties of the two instruments propagated through equation 7, imply closure to within the measurement capabilities. Therefore, most of the $N_2O_5$ was converted into $ClNO_2$, $HNO_3$, and $pNO_3$. Using Table 2 and the calculated

yield values, for example, $N_2O_5$ fractionated for saw palmetto in the high RH (60%) experiment <1% to $ClNO_2$ and 79% to $HNO_3$, or 80% between them, and 28% to $pNO_3$ with ~9% discrepancy. The exception is the one experimental time series shown in Figures 6 and 7, black needlerush at high RH (76%), which exhibits a large (factor of 2.5) negative bias implying a missing source of $pNO_3$. We suspect this indicates a partitioning of excess gas-phase $HNO_3$ from flow reactor surfaces into the BBA at high RH, possibly due to a deliquesced inorganic component. Pre-experiment our instruments sampled the humidified flow through the flow reactor with clean air, however nothing was observed from the walls of the flowtube. As such, we conclude that the bulk of $N_2O_5$ reactivity on BBA that does not lead to Cl-activation produces inorganic $NO_3$, but we are unable to rule out a small amount of particulate organic nitrate production. Molecular analysis of the BBA after $N_2O_5$ processing in future studies could further refine this budget.

**Table 2.** Reactive nitrogen budget measured in the aerosol flow reactor under nocturnal conditions, based on measured changes in $N_2O_5$(g), $HNO_3$(g), $ClNO_2$(g), and particulate nitrate ($pNO_3$). N balance is determined using equation 7. Absolute measurement uncertainty in parentheses.

| Fuel Type | $2\Delta N_2O_5$ (pptv) | $\Delta HNO_3$(g) + $\Delta ClNO_2$ (g) (pptv) | $\Delta pNO_3$ (pptv) | N balance (%) |
|---|---|---|---|---|
| Saw Palmetto LRH | 726 (220) | 321 (100) | 378 (110) | 4 ± 6 |
| Saw Palmetto HRH | 1136 (340) | 911 (270) | 322 (100) | 9 ± 31 |
| Wiregrass LRH | 2843 (850) | 870 (260) | 136 (40) | 65 ± 42 |
| Wiregrass HRH | 2329 (700) | 1086 (330) | 146 (40) | 47 ± 26 |
| Black Needlerush LRH | 2000 (600) | 1204 (360) | 1512 (450) | -35 ± 32 |
| Black Needlerush HRH | 319 (100) | 165 (50) | 957 (290) | -250 ± 78 |
| LL Pine Needles LRH | 2300 (690) | 1054 (316) | 60 (20) | 51 ± 51 |
| LL Pine Needles HRH | 394 (120) | 97 (30) | 100 (30) | 50 ± 19 |

## 4. Conclusions and Atmospheric Implications

In this study the heterogeneous reaction probability of $N_2O_5$(g) ($\gamma(N_2O_5)$) measured on authentic BBA is reported for the first time using controlled aerosol flow reactor experiments. We find $\gamma(N_2O_5)$ to be on the lower end of previous studies using various inorganic and organic aerosols, ranging between 0.002 and 0.006. Even though the BBA particles from certain fuels from this set of experiments contained chloride mass fractions on the higher side compared to other BBA experiments (reported range 0-34%)(2) that should drive $N_2O_5$ reactive uptake and conversion to $ClNO_2$, $ClNO_2$ formation was only detected at significant yields (50%) for the BBA with the highest particle chloride content (22% pCl by mass) at the highest RH used (76%). These results suggest future investigations into the phase state and morphology of BBA that likely play an important role in determining the observed chemical reaction kinetics and product yields.

In our prior related large chamber experiments on BBA reported by Ahern et al, we found that loss of $N_2O_5$ to the chamber walls was too large to allow accurate determination of $\gamma(N_2O_5)$ on BBA(14). On the other hand, in the chamber experiments $ClNO_2$ formation occurred more often than observed in these flow reactor studies and scaled with particulate chloride mass fraction. One possible explanation might involve the humidification and mixing of the chamber leading to a greater potential for deliquescence of inorganic chloride relative to the aerosol flow reactor experiments described here. Moreover, there was greater interaction time between $N_2O_5$ and BBA, and higher aerosol concentrations in the chamber experiments, suggesting that perhaps the $ClNO_2$ formation rate was often below the detection limit given the flow reactor conditions and timescale.

Overall, our results suggest that chloride availability for activation into volatile and reactive chlorine species such as $ClNO_2$ and HCl in fresh BBA is likely reduced, possibly due to the phase state of inorganic salts (e.g. KCl), and particle morphology via organic coatings that hinder heterogeneous reactions between $N_2O_5$ (or $HNO_3$) and chloride. Further work on the deliquescence and efflorescence of inorganic components of authentic BBA that controls the availability of chloride and other components for reaction is likely warranted. Given that we generated and used authentic BBA under atmospherically relevant RH conditions, our results imply that inorganic phase transitions and/or core-shell morphology may well be important in describing the chemical evolution and impacts of atmospheric BBA.

**Conflicts of Interests**

We have no conflicts of interest to declare.

**Acknowledgements**

This work was supported by a grant from the National Science Foundation (NSF) Atmospheric Chemistry Program (AGS-1551981 and AGS-1552608). Authentic biomass fuels were provided by Sara Aicher at Okefenokee National Wildlife Refuge and Rebecca Harrison at Alligator River National Wildlife Refuge.

1. Levin EJTT, McMeeking GR, Carrico CM, Mack LE, Kreidenweis SM, Wold CE, et al. Biomass burning smoke aerosol properties measured during Fire Laboratory at Missoula Experiments (FLAME). 2010 Sep 25;115:D18210. Available from: http://doi.wiley.com/10.1029/2009JD013601
2. McMeeking GR, Kreidenweis SM, Baker S, Carrico CM, Chow JC, Collett JL, et al. Emissions of trace gases and aerosols during the open combustion of biomass in the laboratory. J Geophys Res Atmos. 2009;114(19).
3. Schwier AN, Sellegri K, Mas S, Charrière B, Pey J, Rose C, et al. Primary marine aerosol physical flux and chemical composition during a nutrient enrichment experiment in mesocosms in the Mediterranean Sea. Atmos Chem Phys. 2017;
4. Williams J. Exploring the onset of high-impact mega-fires through a forest land management prism. For Ecol Manage [Internet]. 2013 Apr;294:4–10. Available from: https://linkinghub.elsevier.com/retrieve/pii/S0378112712003593
5. Bond TC, Streets DG, Yarber KF, Nelson SM, Woo JH, Klimont Z. A technology-based global inventory of black and organic carbon emissions from combustion. 2004;109:D14203. Available from: http://doi.wiley.com/10.1029/2003JD003697
6. Crutzen PJ, Andreae MO. Biomass Burning in the Tropics: Impact on Atmospheric Chemistry and Biogeochemical Cycles. Science (80- ) [Internet]. 1990 Dec 21;250(4988):1669–78. Available from: http://www.sciencemag.org/cgi/doi/10.1126/science.250.4988.1669
7. Lu X, Zhang L, Yue X, Zhang J, Jaffe DA, Stohl A, et al. Wildfire influences on the variability and trend of summer surface ozone in the mountainous western United States. Atmos Chem Phys [Internet]. 2016 Nov 24;16(22):14687–702. Available from: https://www.atmos-chem-phys.net/16/14687/2016/
8. Decker ZCJ, Zarzana KJ, Coggon M, Min KE, Pollack I, Ryerson TB, et al. Nighttime Chemical Transformation in Biomass Burning Plumes: A Box Model Analysis Initialized with Aircraft Observations. Environ Sci Technol. 2019;53(5):2529–38.
9. Coggon MM, Veres PR, Yuan B, Koss A, Warneke C, Gilman JB, et al. Emissions of nitrogen-containing organic compounds from the burning of herbaceous and arboraceous biomass: Fuel composition dependence and the variability of commonly used nitrile tracers. Geophys Res Lett [Internet]. 2016 Sep 28;43(18):9903–12. Available from: http://doi.wiley.com/10.1002/2016GL070562
10. Lelieveld J, Crutzen PJ, Dentener FJ. Changing concentration, lifetime and climate forcing of atmospheric methane. 1998 Jan 15;50(2):128–50. Available from: https://www.tandfonline.com/doi/full/10.3402/tellusb.v50i2.16030
11. Brown SS, Ryerson TB, Wollny AG, Brock CA, Peltier R, Sullivan AP, et al. Variability in nocturnal nitrogen oxide processing and its role in regional air quality. Science (80- ). 2006;311(5757):67–70.
12. Dentener FJ, Crutzen PJ. Reaction of N2O5 on tropospheric aerosols: impact on the global distributions of NOx, O3, and OH. J Geophys Res. 1993;98(D4):7149–63.
13. Lobert JM, Keene WC, Logan JA, Yevich R. Global chlorine emissions from biomass burning: Reactive Chlorine Emissions Inventory. 1999 Apr 20;104(D7):8373–89. Available from:

http://doi.wiley.com/10.1029/1998JD100077
14. Ahern AT, Goldberger L, Jahl L, Thornton J, Sullivan RC. Production of N2O5 and ClNO2 through Nocturnal Processing of Biomass-Burning Aerosol. 2018 Jan 16;52(2):550–9. Available from: http://pubs.acs.org/doi/10.1021/acs.est.7b04386
15. Maudlin LCC, Wang Z, Jonsson HHH, Sorooshian A. Impact of wildfires on size-resolved aerosol composition at a coastal California site. Atmos Environ [Internet]. 2015 Oct;119:59–68. Available from: https://linkinghub.elsevier.com/retrieve/pii/S1352231015302843
16. Sarwar G, Simon H, Xing J, Mathur R. Importance of tropospheric ClNO2 chemistry across the Northern Hemisphere. Geophys Res Lett. 2014;41(11):4050–8.
17. Akagi SK, Yokelson RJ, Wiedinmyer C, Alvarado MJ, Reid JS, Karl T, et al. Emission factors for open and domestic biomass burning for use in atmospheric models. Atmos Chem Phys [Internet]. 2011 May 3;11(9):4039–72. Available from: http://www.atmos-chem-phys.net/11/4039/2011/
18. Yokelson RJ, Crounse JD, DeCarlo PF, Karl T, Urbanski S, Atlas E, et al. Emissions from biomass burning in the Yucatan. Atmos Chem Phys [Internet]. 2009 Aug 12;9(15):5785–812. Available from: http://www.atmos-chem-phys.net/9/5785/2009/
19. Van Der Werf GR, Randerson JT, Giglio L, Collatz GJ, Mu M, Kasibhatla PS, et al. Global fire emissions and the contribution of deforestation, savanna, forest, agricultural, and peat fires (1997-2009). Atmos Chem Phys. 2010;10(23):11707–35.
20. Mozurkewich M, Calvert JG. Reaction probability of N2O5 on aqueous aerosols. J Geophys Res. 1988;
21. Van Doren JM, Watson LR, Davidovits P, Worsnop DR, Zahniser MS, Kolb CE. Uptake of N2O5 and HNO3 by aqueous sulfuric acid droplets. J Phys Chem. 1991;
22. Jariyasopit N, Zimmermann K, Schrlau J, Arey J, Atkinson R, Yu TW, et al. Heterogeneous reactions of particulate matter-bound PAHs and NPAHs with NO 3 /N 2 O 5 , OH radicals, and O 3 under simulated long-range atmospheric transport conditions: Reactivity and mutagenicity. Environ Sci Technol. 2014;48(17):10155–64.
23. Kwamena N-OAOA, Abbatt JPDPD. Heterogeneous nitration reactions of polycyclic aromatic hydrocarbons and n-hexane soot by exposure to NO3/NO2/N2O5. Atmos Environ [Internet]. 2008 Nov;42(35):8309–14. Available from: https://linkinghub.elsevier.com/retrieve/pii/S1352231008006638
24. Finlayson-Pitts BJ, Ezell MJ, Pitts JN. Formation of chemically active chlorine compounds by reactions of atmospheric NaCl particles with gaseous N2O5 and ClONO2. Nature [Internet]. 1989 Jan;337(6204):241–4. Available from: http://www.nature.com/articles/337241a0
25. Osthoff HD, Roberts JM, Ravishankara AR, Williams EJ, Lerner BM, Sommariva R, et al. High levels of nitryl chloride in the polluted subtropical marine boundary layer. Nat Geosci [Internet]. 2008 May 6;1(5):324–8. Available from: http://www.nature.com/articles/ngeo177
26. Thornton JA, Abbatt JPD. N2O5 reaction on submicron sea salt aerosol: Kinetics, products, and the effect of surface active organics. J Phys Chem A.

2005;109(44):10004–12.
27. Behnke W, Zetzsch C. Heterogeneous formation of chlorine atoms from various aerosols in the presence of O3 and HCl. J Aerosol Sci [Internet]. 1989 Jan;20(8):1167–70. Available from: https://linkinghub.elsevier.com/retrieve/pii/002185028990788X
28. Hu JH, Abbatt JPD. Reaction Probabilities for N2O5 Hydrolysis on Sulfuric Acid and Ammonium Sulfate Aerosols at Room Temperature. J Phys Chem A. 1997;101(5):871–8.
29. Thornton JA, Braban CF, Abbatt JPD. N2O5 hydrolysis on sub-micron organic aerosols: The effect of relative humidity, particle phase, and particle size. Phys Chem Chem Phys. 2003;5(20):4593–603.
30. Hallquist M, Stewart DJ, Stephenson SK, Cox RA, Anthony Cox R, Cox RA, et al. Hydrolysis of N2O5 on sub-micron sulfate aerosols. Phys Chem Chem Phys [Internet]. 2003;5(16). Available from: http://xlink.rsc.org/?DOI=b301827j
31. Wahner A, Mentel TF, Sohn M, Stier J. Heterogeneous reaction of N2O5 on sodium nitrate aerosol. J Geophys Res Atmos. 1998;103(D23):31103–12.
32. Mentel TF, Sohn M, Wahner A. Nitrate effect in the heterogeneous hydrolysis of dinitrogen pentoxide on aqueous aerosols. Phys Chem Chem Phys [Internet]. 1999;1(24):5451–7. Available from: http://xlink.rsc.org/?DOI=a905338g
33. Bertram TH, Thornton JA. Toward a general parameterization of N2O5 reactivity on aqueous particles: The competing effects of particle liquid water, nitrate and chloride. Atmos Chem Phys. 2009;9(21):8351–63.
34. Behnke W, George C, Scheer V, Zetzsch C. Production and decay of ClNO2 from the reaction of gaseous N2O5 with NaCl solution: Bulk and aerosol experiments. J Geophys Res Atmos. 1997;102(D3):3795–804.
35. Roberts JM, Osthoff HD, Brown SS, Ravishankara AR, Coffman D, Quinn P, et al. Laboratory studies of products of N2O5 uptake on Cl- containing substrates. Geophys Res Lett. 2009;
36. Anttila T, Kiendler-Scharr A, Tillmann R, Mentel TF. On the Reactive Uptake of Gaseous Compounds by Organic-Coated Aqueous Aerosols: Theoretical Analysis and Application to the Heterogeneous Hydrolysis of N 2 O 5. J Phys Chem A [Internet]. 2006 Sep;110(35):10435–43. Available from: https://pubs.acs.org/doi/10.1021/jp062403c
37. Gaston CJ, Thornton JA, Ng NL. Reactive uptake of N2O5 to internally mixed inorganic and organic particles: The role of organic carbon oxidation state and inferred organic phase separations. Atmos Chem Phys. 2014;14(11):5693–707.
38. Heal MR, Harrison MAJJ, Neil Cape J. Aqueous-phase nitration of phenol by N2O5 and ClNO2. Atmos Environ [Internet]. 2007 Jun;41(17):3515–20. Available from: https://linkinghub.elsevier.com/retrieve/pii/S1352231007001355
39. Ryder OS, Campbell NR, Morris H, Forestieri S, Ruppel MJ, Cappa C, et al. Role of Organic Coatings in Regulating N2O5 Reactive Uptake to Sea Spray Aerosol. J Phys Chem A. 2015;119(48):11683–92.
40. Brimblecombe P, Clegg SL. The solubility and behaviour of acid gases in the marine aerosol. J Atmos Chem. 1988;
41. Sullivan RC, Guazzotti SA, Sodeman DA, Tang Y, Carmichael GR, Prather KA. Mineral dust is a sink for chlorine in the marine boundary layer. Atmos Environ

[Internet]. 2007 Nov;41(34):7166–79. Available from: https://linkinghub.elsevier.com/retrieve/pii/S1352231007004864

42. Laskin A, Moffet RC, Gilles MK, Fast JD, Zaveri RA, Wang B, et al. Tropospheric chemistry of internally mixed sea salt and organic particles: Surprising reactivity of NaCl with weak organic acids. 2012 Aug 16;117:n/a-n/a. Available from: http://doi.wiley.com/10.1029/2012JD017743
43. Thornton JA, Kercher JP, Riedel TP, Wagner NL, Cozic J, Holloway JS, et al. A large atomic chlorine source inferred from mid-continental reactive nitrogen chemistry. Nature [Internet]. 2010 Mar;464(7286):271–4. Available from: http://www.nature.com/articles/nature08905
44. Mielke LH, Furgeson A, Osthoff HD. Observation of ClNO2 in a mid-continental urban environment. Environ Sci Technol. 2011;45(20):8889–96.
45. Braun RA, Dadashazar H, Macdonald AB, Aldhaif AM, Maudlin LC, Crosbie E, et al. Impact of Wildfire Emissions on Chloride and Bromide Depletion in Marine Aerosol Particles. 2017 Aug 15;51(16):9013–21. Available from: http://pubs.acs.org/doi/10.1021/acs.est.7b02039
46. Jathar SH, Gordon TD, Hennigan CJ, Pye HOT, Pouliot G, Adams PJ, et al. Unspeciated organic emissions from combustion sources and their influence on the secondary organic aerosol budget in the United States. Proc Natl Acad Sci [Internet]. 2014 Jul 22;111(29):10473–8. Available from: http://www.pnas.org/cgi/doi/10.1073/pnas.1323740111
47. Ortega AM, Day DA, Cubison MJ, Brune WH, Bon D, de Gouw JA, et al. Secondary organic aerosol formation and primary organic aerosol oxidation from biomass-burning smoke in a flow reactor during FLAME-3. Atmos Chem Phys [Internet]. 2013 Nov 28;13(22):11551–71. Available from: https://www.atmos-chem-phys.net/13/11551/2013/
48. Bian Q, May AA, Kreidenweis SM, Pierce JR. Investigation of particle and vapor wall-loss effects on controlled wood-smoke smog-chamber experiments. Atmos Chem Phys [Internet]. 2015 Oct 6;15(19):11027–45. Available from: https://www.atmos-chem-phys.net/15/11027/2015/
49. Grieshop AP, Logue JM, Donahue NM, Robinson AL. Laboratory investigation of photochemical oxidation of organic aerosol from wood fires 1: measurement and simulation of organic aerosol evolution. Atmos Chem Phys [Internet]. 2009 Feb 18;9(4):1263–77. Available from: http://www.atmos-chem-phys.net/9/1263/2009/
50. Cubison MJ, Ortega AM, Hayes PL, Farmer DK, Day D, Lechner MJ, et al. Effects of aging on organic aerosol from open biomass burning smoke in aircraft and laboratory studies. Atmos Chem Phys [Internet]. 2011 Dec 5;11(23):12049–64. Available from: https://www.atmos-chem-phys.net/11/12049/2011/
51. Abbatt JPD, Lee AKY, Thornton JA. Quantifying trace gas uptake to tropospheric aerosol: Recent advances and remaining challenges. Vol. 41, Chemical Society Reviews. 2012. p. 6555–81.
52. Gaston CJ, Thornton JA. Reacto-Diffusive Length of N2O5 in Aqueous Sulfate- and Chloride-Containing Aerosol Particles. J Phys Chem A. 2016;120(7):1039–45.
53. Pósfai M, Simonics R, Li J, Hobbs P V., Buseck PR. Individual aerosol particles from biomass burning in southern Africa: 1. Compositions and size distributions of carbonaceous particles. J Geophys Res D Atmos. 2003;

54. Li X, Gupta D, Eom H-JJ, Kim HK, Ro C-UU. Deliquescence and efflorescence behavior of individual NaCl and KCl mixture aerosol particles. Atmos Environ [Internet]. 2014 Jan;82:36–43. Available from: https://linkinghub.elsevier.com/retrieve/pii/S1352231013007644
55. Zauscher MD, Wang Y, Moore MJK, Gaston CJ, Prather KA. Air quality impact and physicochemical aging of biomass burning aerosols during the 2007 San Diego wildfires. Environ Sci Technol. 2013;
56. Pratt KA, Murphy SM, Subramanian R, Demott PJ, Kok GL, Campos T, et al. Flight-based chemical characterization of biomass burning aerosols within two prescribed burn smoke plumes. Atmos Chem Phys. 2011;
57. Silva PJ, Liu DY, Noble CA, Prather KA. Size and chemical characterization of individual particles resulting from biomass burning of local Southern California species. Environ Sci Technol. 1999;
58. Alvarado M, Gonzalez F, Fletcher A, Doshi A. Towards the development of a low cost airborne sensing system to monitor dust particles after blasting at open-pit mine sites. Sensors (Switzerland). 2015;15(8):19703–23.
59. Li J, Pósfai M, Hobbs P V., Buseck PR. Individual aerosol particles from biomass burning in southern Africa: 2. Compositions and aging of inorganic particles. J Geophys Res D Atmos [Internet]. 2003 Jul 16;108(D13):n/a-n/a. Available from: http://doi.wiley.com/10.1029/2002JD002310
60. Ahern AT, Subramanian R, Saliba G, Lipsky EM, Donahue NM, Sullivan RC. Effect of secondary organic aerosol coating thickness on the real-time detection and characterization of biomass-burning soot by two particle mass spectrometers. Atmos Meas Tech [Internet]. 2016 Dec 22;9(12):6117–37. Available from: https://www.atmos-meas-tech.net/9/6117/2016/
61. Liu PSK, Deng R, Smith KA, Williams LR, Jayne JT, Canagaratna MR, et al. Transmission efficiency of an aerodynamic focusing lens system: Comparison of model calculations and laboratory measurements for the aerodyne aerosol mass spectrometer. Aerosol Sci Technol. 2007;
62. Brown SS, Stutz J. Nighttime radical observations and chemistry [Internet]. Chemical Society Reviews 2012 p. 6405–47. Available from: http://xlink.rsc.org/?DOI=c2cs35181a
63. Wagner NL, Dubé WP, Washenfelder RA, Young CJ, Pollack IB, Ryerson TB, et al. Diode laser-based cavity ring-down instrument for NO3, N2O5, NO, NO2 and O3 from aircraft. Atmos Meas Tech. 2011;4(6):1227–40.
64. McNeill VF, Patterson J, Wolfe GM, Thornton JA. The Effect of Varying Levels of Surfactant on the Reactive Uptake of N2O5 to Aqueous Aerosol. Atmos Chem Phys. 2006;6(6):1635–44.
65. Lee BH, Lopez-Hilfiker FD, Schroder JC, Campuzano-Jost P, Jimenez JL, McDuffie EE, et al. Airborne Observations of Reactive Inorganic Chlorine and Bromine Species in the Exhaust of Coal-Fired Power Plants. J Geophys Res Atmos. 2018;
66. Lee BH, Lopez-Hilfiker FD, Mohr C, Kurtén T, Worsnop DR, Thornton JA. An iodide-adduct high-resolution time-of-flight chemical-ionization mass spectrometer: Application to atmospheric inorganic and organic compounds. Environ Sci Technol. 2014;48(11):6309–17.

67. Fuchs N. A, Sutugin A. G. Coagulation rate of highly dispersed aerosols. J Colloid Sci [Internet]. 1965 Aug;20(6):492–500. Available from: https://linkinghub.elsevier.com/retrieve/pii/0095852265900310
68. Hanson D, Kosciuch E. The NH3 mass accommodation coefficient for uptake onto sulfuric acid solutions. 2003 Apr;107(13):2199–208. Available from: https://pubs.acs.org/doi/10.1021/jp021570j
69. Badger CL, Griffiths PT, George I, Abbatt JPD, Cox RA. Reactive uptake of N2O5 by aerosol particles containing mixtures of humic acid and ammonium sulfate. J Phys Chem A. 2006;110(21):6986–94.
70. Mochida M, Kawamura K. Hygroscopic properties of levoglucosan and related organic compounds characteristic to biomass burning aerosol particles. 2004 Nov 16;109:n/a-n/a. Available from: http://doi.wiley.com/10.1029/2004JD004962
71. Karagulian F, Santschi C, Rossi MJ. The heterogeneous chemical kinetics of N2O5 on CaCO3 and other atmospheric mineral dust surrogates. Atmos Chem Phys. 2006;6(5):1373–88.
72. Brown SS, Dubé WP, Fuchs H, Ryerson TB, Wollny AG, Brock CA, et al. Reactive uptake coefficients for N2O5 determined from aircraft measurements during the Second Texas Air Quality Study: Comparison to current model parameterizations. J Geophys Res Atmos. 2009;114(11).
73. Bertram TH, Thornton JA, Riedel TP, Middlebrook AM, Bahreini R, Bates TS, et al. Direct observations of N2O5 reactivity on ambient aerosol particles. Geophys Res Lett. 2009;36(19).
74. Riedel TP, Bertram TH, Ryder OS, Liu S, Day DA, Russell LM, et al. Direct N2O5 reactivity measurements at a polluted coastal site. Atmos Chem Phys. 2012;12(6):2959–68.
75. Tham YJ, Wang Z, Li Q, Wang W, Wang X, Lu K, et al. Heterogeneous N2O5 uptake coefficient and production yield of ClNO2 in polluted northern China: roles of aerosol water content and chemica. Atmos Chem Phys [Internet]. 2018 Sep 12;18(17):13155–71. Available from: https://www.atmos-chem-phys.net/18/13155/2018/
76. Petters MD, Carrico CM, Kreidenweis SM, Prenni AJ, DeMott PJ, Collett JL, et al. Cloud condensation nucleation activity of biomass burning aerosol. J Geophys Res Atmos. 2009;
77. Engelhart GJ, Hennigan CJ, Miracolo MA, Robinson AL, Pandis SN. Cloud condensation nuclei activity of fresh primary and aged biomass burning aerosol. Atmos Chem Phys. 2012;
78. Carrico CM, Petters MD, Kreidenweis SM, Sullivan AP, McMeeking GR, Levin EJT, et al. Water uptake and chemical composition of fresh aerosols generated in open burning of biomass. Atmos Chem Phys. 2010;
79. Ahn KH, Kim SM, Jung HJ, Lee MJ, Eom HJ, Maskey S, et al. Combined use of optical and electron microscopic techniques for the measurement of hygroscopic property, chemical composition, and morphology of individual aerosol particles. Anal Chem. 2010;82(19):7999–8009.
80. Freney EJ, Martin ST, Buseck PR. Deliquescence and efflorescence of potassium salts relevant to biomass-burning aerosol particles. Aerosol Sci Technol [Internet]. 2009 Jul 6;43(8):799–807. Available from:

http://www.tandfonline.com/doi/abs/10.1080/02786820902946620

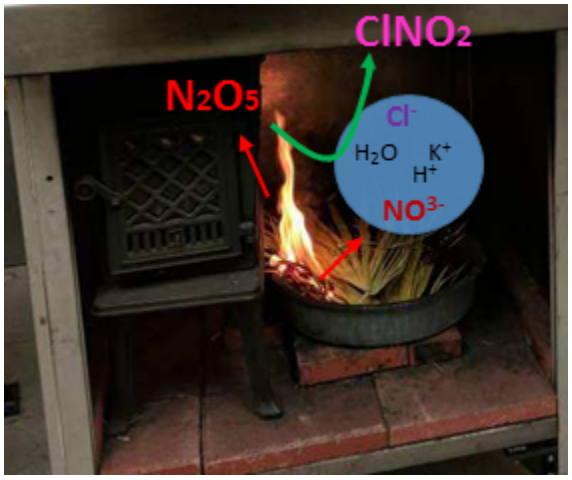
ClNO2
N2O5
Cl-
H2O
K+
H+
NO3-